# Elastic cost of silicon step rebonding

F. Leroy,[1,*] Y. Garreau,[2,3] F. Cheynis,[1] B. Croset,[4] A. Coati,[3] P. Müller,[1] and G. Prévot[4]

[1]*Aix Marseille Université, CINaM UMR 7325, Campus de Luminy, Case 913, F-13288 Marseille Cedex, France*

[2]*Université Paris Diderot, Sorbonne-Paris-Cité, MPQ, UMR 7162 CNRS, Bâtiment Condorcet, Case 7021, 75205 Paris Cedex 13, France*

[3]*Synchrotron SOLEIL, l'Orme des Merisiers, Saint-Aubin, B.P. 48, 91192 Gif sur Yvette Cedex, France*

[4]*Sorbonne Universités, UPMC Univ Paris 06, CNRS-UMR 7588, Institut des NanoSciences de Paris, F-75005 Paris, France*

(Received 17 November 2015; published 15 January 2016)

We study by grazing incidence x-ray diffraction the strain field induced by periodic double steps on a Si(1 1 15) surface that is a vicinal of a Si(001) surface misoriented by 5.4° towards the ⟨110⟩ direction. The best fit of the experimental structure factors is reached on the basis of the rebonded $D_B$ step edge model and the displacement field is well characterized assuming that steps are described by parallel rows of extended buried elastic dipoles. The dipole characteristics are the dipole position with respect to the step edge, the dipole amplitude ($2.0 \pm 0.5$ nN), and the lever arm $\Omega = 5.3°$ and force $\Phi = 3.7°$ orientations. We show that the dipole is dominated by a large stretch component localized between the lower and the upper corners of the step, which we assign to the presence of the rebonded atom at the step.

DOI: 10.1103/PhysRevB.93.045416

## I. INTRODUCTION

Due to their huge technological interest for the development of microelectronics, Si surfaces have been extensively studied. A large number of advanced experimental tools have been used for the precise characterization of these surfaces under equilibrium [1–3] or growth [4,5] conditions. These studies have shown that Si surface properties, e.g., surface energy and surface stress, are intimately related to the structure of terraces and step edges [6–8]. Moreover, it has been shown from real-time studies that kinetic mechanisms such as adsorption [9] and thin-film growth [5] occur mainly at step edges. Understanding step properties is thus crucial from the perspective of better control of growth processes.

The Si(001) surface is probably one of the most studied. Despite this effort, there have been only a few studies devoted to the description of the step energy and, more particularly, of step-step interactions. Since the atoms that belong to the step edges have a different number of nearest neighbors than the bulk atoms, steps give rise to a lattice distortion that mediates step-step interaction. Marchenko and Parshin [10,11] showed in the eighties that the displacement field induced by surface steps in the underlying bulk can be calculated in the framework of elasticity theory. They proposed to model steps as a periodic array of one-dimensional (1D) lines of elastic dipoles acting on the surface plane of a semi-infinite substrate. However, if the Marchenko and Parshin model gives a general framework for the description of step-step interactions in terms of dipole-dipole elastic interactions, it cannot account for the atomic details at the step edge and an atomistic approach is needed to quantitatively unravel the dipole characteristics. From that perspective a model of buried dipoles lines with out-of-plane lever arms has been proposed and checked by grazing incidence x-ray diffraction (GIXD) [12–15]. The crystal truncation rods (CTRs) of regular vicinal surfaces have specific modulations arising from the elastic displacement field induced by surface steps. Fitting the buried dipole model to the experimental structure factor data allows extraction of the parameters, i.e., the spatial localization, amplitude, torque and stretch components, and lever arm orientation of the dipole with respect to the surface plane [15]. These experimental results can be compared with calculations based on semiempirical potentials [16,17] or *ab initio* methods [18]. This approach has been successfully used for vicinal surfaces of many metals [13,19,20] and has also been recently applied to the case of a Si(111) vicinal surface [21].

This article aims to address the step-step interactions on the most meaningful Si surface for its technological relevance, the Si(001) surface. Beyond this aspect, Si(001) has been chosen because (i) Si single crystals can be grown defect free, (ii) vicinal surfaces of Si(001) may be prepared to reach the quasiperfect long-range periodicity necessary to get valuable diffraction data, and (iii) the crystallographic structures and surface reconstructions of Si(001) vicinal surfaces are well documented [1]. Moreover, due to the diamond structure of Si, steps on a vicinal surface of Si(001) may bear monopoles or dipoles according to the miscut angle with respect to the nominal crystallographic plane orientation. In Ref. [21] we report the case of a Si(7 7 10) surface, which is a vicinal of Si(111). Due to the matching of the step periodicity with the $(7 \times 7)$ surface reconstruction on (111) terraces, the Si(7 7 10) surface spontaneously forms a triple-step structure. In order to achieve a better understanding of step interactions on Si(001), this article focuses on the description of the Si(1 1 15) surface, which is a vicinal of the Si(001) surface with double steps aligned along the $[1\bar{1}0]$ direction.

## II. DESCRIPTION OF THE SURFACE

The structure of stepped Si(001) surfaces has been widely studied and is now well documented [1,16,22]. When a perfect flat Si(001) is obtained by a cleavage process dangling bonds are created. The number of dangling bonds is reduced by the formation of dimers aligned along the ⟨110⟩ direction forming a pattern of dimer rows. Due to the diamond structure of silicon, two neighboring terraces separated by an atomic step have different surface terminations: one terrace

*leroy@cinam.univ-mrs.fr

 

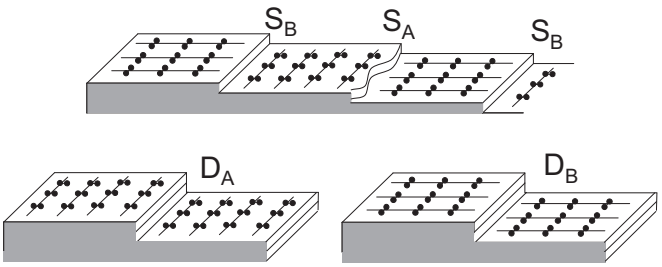


FIG. 1. Scheme of the surface termination of vicinal surfaces of Si(001). Step edges are oriented in the $\langle 1\bar{1}0\rangle$ direction. For vicinal angles larger than 3.5° the surface evolves from single step ($a_0/4$) to double step ($a_0/2$). See text for details.

exhibits a (1 × 2) reconstructed surface with dimers parallel to the $[\bar{1}10]$ direction, while the other terrace exhibits a (2 × 1) reconstructed surface with dimers parallel to the [110] direction (see Fig. 1). Therefore it is known that (i) two types of monoatomic steps exist on a Si(001) vicinal surface: the $S_A$ steps, where the upper terrace forms dimers perpendicular to the step edge, and the $S_B$ steps, where the upper terrace forms dimers parallel to the step edge; and (ii) that the surface stress tensors of two neighboring terraces are second rank tensor which reads $\begin{pmatrix} s_\parallel & 0 \\ 0 & s_\perp \end{pmatrix}$ for one terrace and $\begin{pmatrix} s_\perp & 0 \\ 0 & s_\parallel \end{pmatrix}$ for the other one [23].

For a vicinal angle larger than 3.5° towards the $\langle 110\rangle$ axis, there is a transition from a surface formed by single $S_A$ and $S_B$ steps towards a surface formed by double steps (see Fig. 1) [17,22,24]. Again, two types of double steps may exist: $D_A$ double steps, which separate two equivalent terraces with dimers perpendicular to the step edge; and $D_B$ double steps, which separate two equivalent terraces with dimers parallel to the step edge. $D_B$ steps are energetically more favorable than $D_A$ steps [1,16].

Following Alerhand *et al.* [23], the surface stress discontinuity at the edge of a monoatomic step aligned in the $[1\bar{1}0]$ direction on vicinal surfaces of Si(001) gives rise to a line of force monopoles localized at the step edges and proportional to the surface stress anisotropy $\pm|s_\parallel - s_\perp|$. The result is that steps interact through the bulk displacement field and the step-step interaction energy per unit length scales as $\ln(d)$, where $d$ is the step-step distance.

For a double step, the edge separates two equivalent terraces, therefore it bears not a line of force monopoles, but a line of force dipoles [6]. The result is that the interactions between double steps on Si are dominated by dipole-dipole interactions and the energy per unit length decays more rapidly as $1/d^2$. Contrary to single-step interactions, which

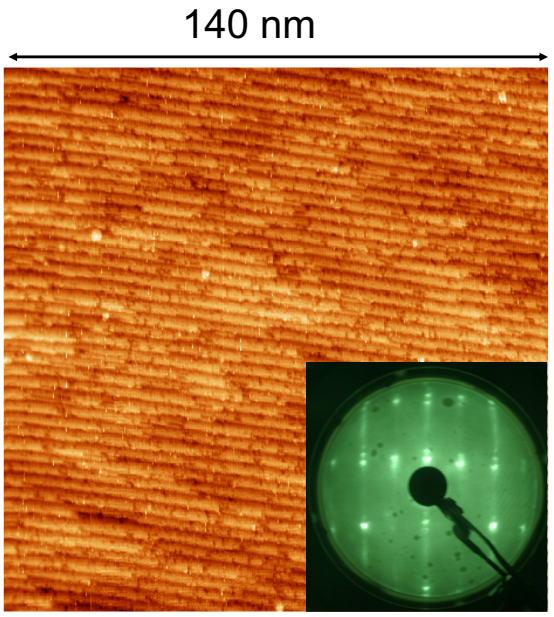


FIG. 2. Scanning tunneling microscopy image of Si(1 1 15). The quasiperfect long-range order of double steps is clear. Inset: Corresponding LEED pattern ($E = 59.3$ eV). Satellite spots around the Bragg peaks show the long-range order of the steps.

are dominated by the surface stress discontinuity between adjacent terraces, the exact atomic arrangement at the step edge of double steps strongly affects the dipole characteristics (position, amplitude, orientation, etc.) and thus the step-step interactions. If calculations and experimental works have been performed to extract the surface stress anisotropy from single steps on Si(001) (see Table I), only scarce numerical studies [17,24,25] have undertaken the dipole-dipole interactions of double steps on Si(001) and no experimental studies have been reported. This absence of data is mainly due to the difficult evaluation in real space (scanning probe microscopy) of the step fluctuations (terrace width distribution) to extract the interaction potential. Measurement of the displacement field induced by steps by x-ray diffraction appears to be a much more direct approach [12–15]. To tackle the question of double-step interactions on Si(001), we have selected a Si(1 1 15) surface. This is a vicinal of Si(001) with a miscut angle of 5.4° towards $[1\bar{1}0]$. The Si(1 1 15) surface was prepared *ex situ* first by a chemical cleaning, then by degassing in an ultrahigh vacuum during 6 h at 500°C by radiation heating to avoid electromigration effects, and, finally, heated at 1250°C during 30 s before going back to room temperature. Figure 2 shows a typical scanning tunneling microscopy

TABLE I. Calculated values of surface stress components ($\mathrm{Nm}^{-1}$) for a Si(001) surface. Experimental surface stress anisotropy values are listed in the last row.

| | Haiss *et al.* [26] | Payne *et al.* [27] | Mead *et al.* [28] | Poon *et al.* [17] | Garcia *et al.* [29] | Umeno *et al.* [30] | Miyamoto *et al.* [31] | Hara *et al.* [32] | Delph [33] | Hecquet [34] |
|---|---|---|---|---|---|---|---|---|---|---|
| $s_{\parallel,\mathrm{theory}}$ | 0.51 | 0.75 | 1.70 | 1.18 | 2.38 | 1.284 | 0.75 or 1.11 | 0.73 or 0.40 | 0.13 | 0.41 |
| $s_{\perp,\mathrm{theory}}$ | 1.25 | −2.11 | −0.96 | −0.05 | −0.86 | −0.286 | −1.19 or −0.4 | −1.06 or −1.34 | −1.12 | −1.1 |
| $\lvert s_\parallel - s_\perp\rvert_{\mathrm{expt}}$ | | 1.12 [23] | | | | 0.56 [22] | | 1.28–2.08 [35] | | |

image recorded at room temperature. The prepared surface is formed of $D_B$ double steps periodically separated by $(1 \times 2)$ reconstructed terraces (width, 2.89 nm). The surface presents a quasiperfect long-range order (see LEED pattern in inset in Fig. 2) as expected for GIXD experiments.

### III. X-RAY DIFFRACTION MEASUREMENTS

The x-ray diffraction measurements were performed in an ultrahigh vacuum chamber coupled with a $z$-axis diffractometer at the BM32 beamline of the European Synchrotron Radiation Facility [36]. CTRs were measured under a grazing incidence angle ($\alpha = 0.1°$) at $\lambda = 0.0689$ nm ($E = 18$ keV). GIXD measurements were performed at room temperature with a residual gas pressure lower than $10^{-10}$ mb. A total of 1158 structure factors were measured along 14 CTRs. The integrated intensities were collected with a Maxipix 2D detector in stationary mode [37]. To describe the surface structure we use the Si(1 1 15) surface unit cell $(\vec{a}, \vec{b}, \vec{c})$ in the direct space defined by $\vec{a} = 1/2[-15\ -15\ 1]$, $\vec{b} = 1/2[1\ -1\ 0]$, and $\vec{c} = [1\ 1\ 15]$, where the indices refer to the *fcc* unit cell. The reciprocal-space transformation from the surface coordinates $(h,k,l)$ to the standard *fcc* coordinates $(H,K,L)$ is given by

$$\begin{pmatrix} H \\ K \\ L \end{pmatrix} = \frac{1}{227} \begin{pmatrix} -15 & 227 & 1 \\ -15 & -227 & 1 \\ 2 & 0 & 15 \end{pmatrix} \begin{pmatrix} h \\ k \\ l \end{pmatrix}.$$

We have found that the experimental CTRs are parallel to the macroscopic surface orientation, which indicates that no macroscopic faceting occurs.

### IV. MODEL AND EXPERIMENTAL RESULTS

We first need a preliminary accurate description of the ideal vicinal surface we use (which means without the step-induced strain field). The atomic positions on a stepped Si(001) surface have been measured by many authors [1,22,38]. It is has been shown, in particular, that $D_B$ step edges are characterized by dangling bonds that can be reduced by incorporating extra atoms at the edge to form rebonded steps (Fig. 3). These extra atoms reduce the total energy but enhance the surface stress perpendicular to the step edges [1]. These positions have been used as initial conditions, then have been relaxed in the fitting process.

We have used a least-squares fitting procedure based on the Levenberg-Marquardt algorithm and the following definition of $\chi^2$ [39]:

$$\chi^2 = \frac{1}{N_{\rm pt} - N_{\rm par}} \sum^{N_{\rm pt}} \left( \frac{F_{\rm th} - F_{\rm exp}}{\sigma_{\rm exp}} \right)^2,$$

where $F_{\rm exp}$ and $F_{\rm th}$ are the experimental and theoretical structure factors, $\sigma_{\rm exp}$ is the associated experimental uncertainty, $N_{\rm par}$ the number of free parameters, and $N_{\rm pt}$ the total number of data points.

The experimental structure factors as well as the best fits are reported in Fig. 4. The overall agreement on all CTRs shows that the $D_B$ step model accurately describes the atomic positions without relaxations. Moreover, rapid evolutions of the structure factors perpendicular to the surface are measured. This indicates already that large atomic displacements with respect to the unstrained state occur deep in the Si bulk. In particular, important variations of the diffracted intensity in a narrow $L$ range are observed at specific positions of the reciprocal space. Elastic displacements due to the steps give rise to specific features on CTRs on both sides of Bragg peaks [15]. For a given vicinal surface, the position of these satellites can be calculated from the wave vector of the elastic waves. For Si(1 1 15) the first-order elastic modes we calculate from Ref. [14] using the Si elastic constants correspond to positions at $\pm(2\,0\ -1.34)$ and $\pm(2\,0\,1.17)$ from the Bragg peaks. In the collected data, these elastic contributions should thus be visible, for instance, on the $(-12\ 0\ L)$ and $(-14\ 0\ L)$ rods, respectively, close to $L = 17$ and $L = 47$. As a matter of fact, strong accidents are clearly visible at these calculated positions on the corresponding CTRs in Fig. 4. Far from these regions of the reciprocal space, the elastic contribution is weaker and the structure factor evolution is mainly affected by the atomic structure of the surface. This is indeed what is observed.

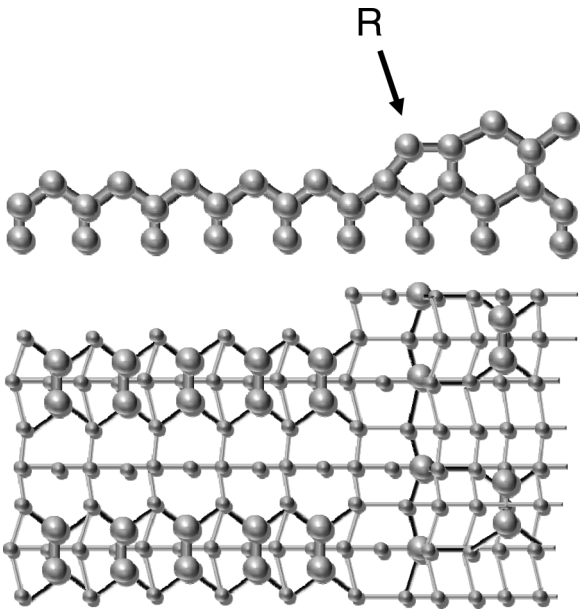


FIG. 3. Scheme of the atom positions at $D_B$ steps of Si(001). The black arrow indicates the rebonded atom position R at the step edge.

In Fig. 5(a) we sketch the geometrical characteristics of an extended dipole with respect to the vicinal surface. The two points of the dipole at the $D_B$ step edge are assumed to be located at $(x_1,z_1)$ and $(x_2,z_2)$ from the upper corner of the step with respect to the macroscopic vicinal surface. The forces on the dipole can be decomposed into two components: a stretch component $F_S$ along the dipolar line (along the two blue points) and a torque component $F_T$ in the perpendicular direction. By definition, a compressive (tensile) stretch dipole component corresponds to a positive (negative) value of $P_S$. The torque effect is a tendency to rotate the direction of the dipolar line. A positive value of $P_T$ corresponds to a rotation of the dipolar line clockwise, and a negative value to a counterclockwise rotation. In the case in Fig. 5 positive (respectively negative) values of $P_T$ correspond to an inward (outward) rotation of the step (dotted line). The $\Omega$ angle corresponds to the angle

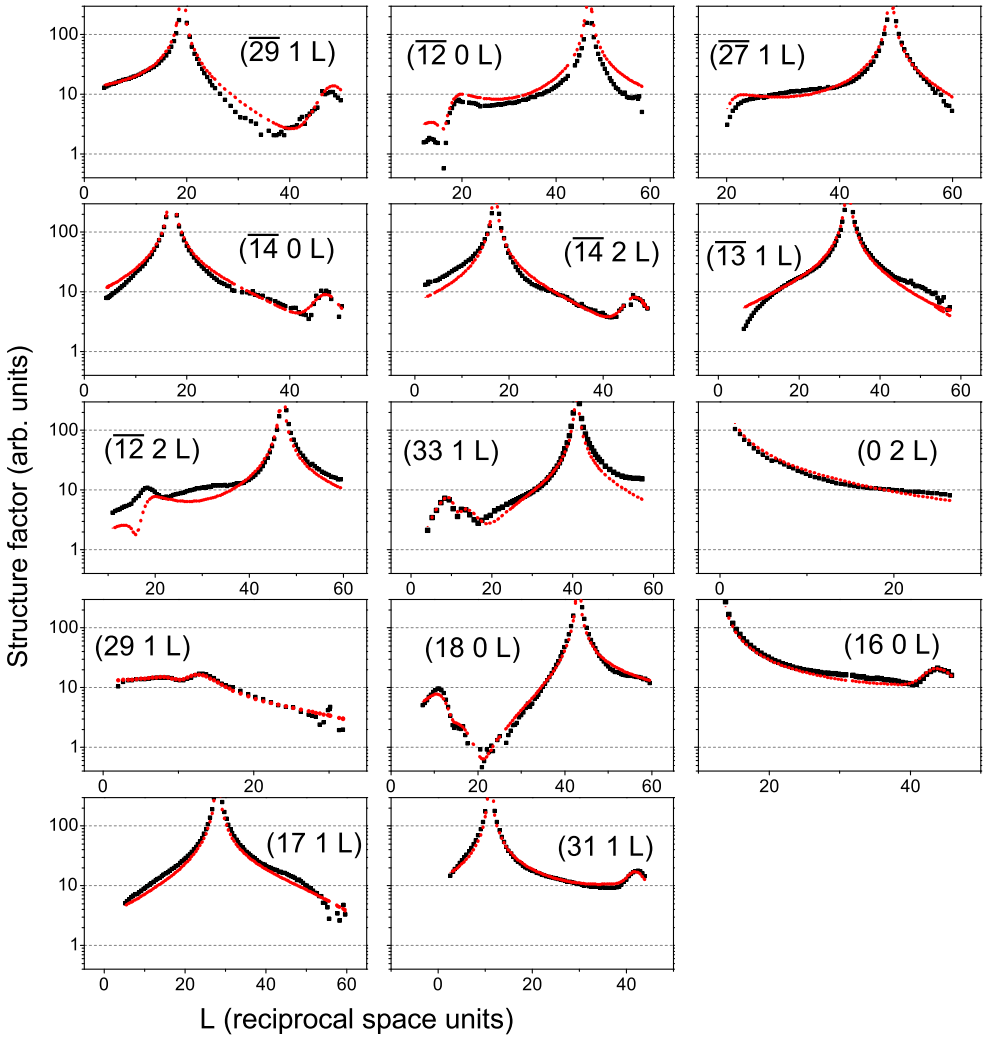


FIG. 4. Experimental structure factors (black circles) and best fit [dashed (red) line] to the extended dipole model.

between the macroscopic vicinal surface and the dipolar line, while the $\Phi$ angle characterizes the angle of force $F$ with respect to the dipolar line. Obviously the amplitude of the dipole $P$ is given by $P = \sqrt{P_S^2 + P_T^2}$.

The experimental results can well be fitted by the rebonded $D_B$ model associated with a buried extended dipole whose characteristics are reported in Figs. 5(a) and 5(b) and Table II. Note that the model has a small positive torque component and a large and positive stretch component. We also report in Fig. 6 the displacement fields of the dipole configuration. Figure 6(a) shows the displacement vectors; arrows correspond to the local values $\times 100$ to increase the visibility. To display the whole structure of the displacement field deep into the bulk (vortex effect) it is represented by lines in Fig. 6(b) to show the direction of the displacement field at each point.

## V. DISCUSSION

The step description in terms of the dipolar distribution is valid since we have been able to fit the structure factors and, especially, the elastic features close to the Bragg peaks. The extended dipole model provides two coherent positions for the forces: $(x_1, z_1)$ and $(x_2, z_2)$ [see Fig. 5(b) and Table II ], which correspond, respectively, to Si atom positions at the lower and upper corners of the step edge. In order to analyze this model let us first consider the details of the dipole geometry. As the angle between the lever arm of the dipole and the force is very small ($\Phi = 3.7°$; see Table II) the dipole is dominated by the stretch component $P_S = 2.0 \pm 0.5$ nN. We can estimate the stress of the step $\tau$ as the ratio of the stretch component of the dipole to the lever arm length ($1.15 \times a_0$). It results that $\tau = 3.25 \pm 0.80$ Nm$^{-1}$. We can infer that this large stress on the step edge results from the rebonded atom at the step edge, which decreases the total energy by reducing the number of dangling bonds at the expense of a large stretch stress at the step. Considering now the local torque component $P_T$ of the dipole ($0.13 \pm 0.05$ nN) it is rather small and plays a minor role in the energetics of the step. Nevertheless, assuming that the lever arm of the dipole is in the surface plane, and following Marchenko and Parshin [11], a torque component $P_T = sh$ must be associated with the height discontinuity, $h$, of the surface stress component, $s$, of the nominal surface normal to the step direction [6]. We can estimate the surface stress knowing the double-step height. The extracted surface stress value $s_\perp = 0.48$ Nm$^{-1}$ is small and positive, whereas the calculated ones are negative (see Table I). However, one

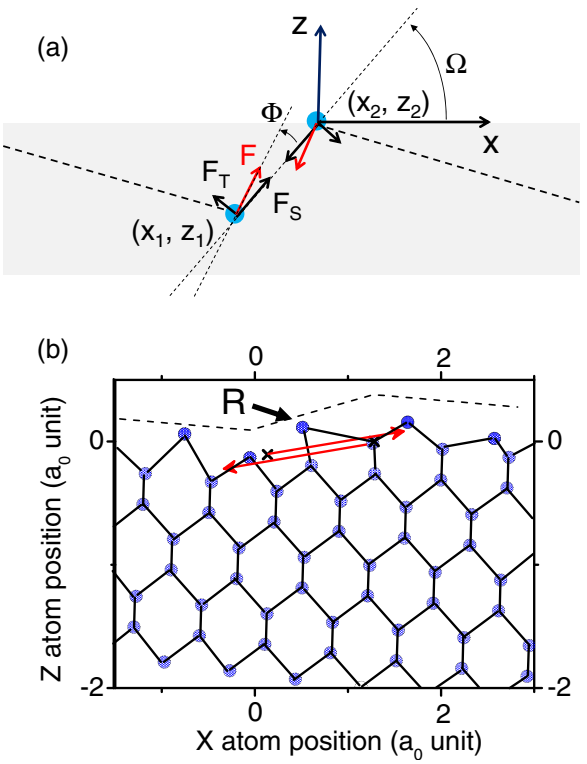


FIG. 5. (a) Scheme of the extended dipole model. (b) Closed view of the calculated atomic positions around the step edge obtained from the fit of the structure factors. The positions of the two forces derived from the extended dipole model are very close, respectively, to the upper and lower corners of the step edge (around the rebonded atom). Note the large displacement in the $(x,z)$ plane of the rebonded atom R.

must remember that the $P_T = sh$ relation originates from the mechanical equilibrium (no global torque) between the forces induced by the surface stress and the local forces created at the step edge responsible for the elastic relaxations. Moreover, the surface stress on a terrace is well defined only far from the step. It is obviously valid for a single step separating two extended terraces but becomes questionable for high miscut angles, i.e., when the terrace and the step widths are similar. In the case under study, the terrace width is only 10 times larger than the step width and we can infer that the rebonding at the double-step edge modifies the surface stress.

Let us now consider the elastic interaction between steps. Since the Marchenko and Parshin work [11] it is known that this interaction energy scales as $A_{\rm el}/d^2$, where $d$ is the step-

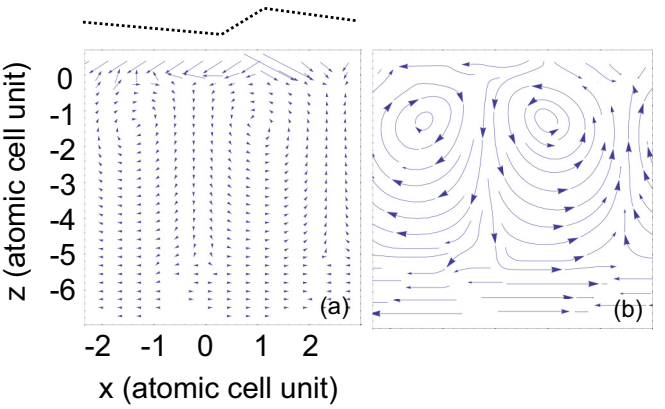


FIG. 6. Cross sections of the displacement fields. The free surface is on top (scheme of the step). (a) For clarity the displacements have been multiplied by 100. (b) The displacement field and its vortex structure are highlighted by lines that show the local direction of the displacement field.

step distance. For $\Omega \neq 0$, the interaction energy assuming an isotropic crystal depends on the relative orientation of the force component with respect to the lever arm [14,40] as

$$A_{\rm el} = \frac{2}{\pi E} P^2 \Big[ (1-\nu^2) - \frac{(1-\nu^2)(1-2\nu)}{(1-\nu)^2} \sin^2(\Phi-\Omega) \times \sin^2(\Omega) + \frac{1}{2}(1+\nu)\sin(2(\Phi-\Omega))\sin(2\Omega) \Big]. \quad (1)$$

Using the Young modulus $E = 0.16 \times 10^{12}$ Nm$^{-2}$ and Poisson ratio $\nu = 0.22$ of polycrystalline silicon [41] and the values of $P$, $\Omega$, and $\Phi$ from Table II we obtain $A_{\rm el} = 1.58 \times 10^{-29}$ J m. If we take fully into account the crystal anisotropy (see Eq. (47) in Ref. [14]) and use the stiffness tensor coefficients of Si ($C_{11} = 1.65 \times 10^{11}$ Pa, $C_{12} = 0.64 \times 10^{11}$ Pa, $C_{44} = 0.80 \times 10^{11}$ Pa), we obtain a slightly smaller value, $A_{\rm el} = 1.14 \times 10^{-29}$ Jm. No experimental data from the literature are available to validate this result but it can be compared to scarce numerical calculations based on the empirical potential using either the Stillinger-Weber potential [17] or the extended Brenner potential [24]. Based on the rebonded $D_B$ model and calculating the interaction energy as a function of the step-step distance these models provide an estimate of the prefactor $A_{\rm el}$ which depends on local details of the step structure. Both models give much higher interaction energies (respectively, $A_{\rm el} = 8.7 \times 10^{-29}$ Jm [17] and $A_{\rm el} = 6.9 \times 10^{-29}$ Jm [24]). This discrepancy can arise from the limited size of the computational unit cell's preventing the surface from being fully relaxed. Moreover, local relaxations

TABLE II. Dipole parameters: $x_1$, $z_1$, $x_2$, and $z_2$ are the in-plane and out-of-plane positions of the two forces of the dipole [in $a_0$ units, where $a_0 = 5.431$ Å is the lattice parameter of Si(001)]. $F_x$ and $F_z$ are the forces applied at atomic positions $x_1$ and $z_1$, per unit of atom ($\frac{a_0}{\sqrt{2}}$), and projected onto $x$ and $y$ coordinates (nN). $P_S$ and $P_T$ are the torque dipole density components.

| | Position 1 | | Position 2 | | Force | | Dipole (nN) | | Angle (deg) | |
|---|---|---|---|---|---|---|---|---|---|---|
| | $x_1$ | $z_1$ | $x_2$ | $z_2$ | $F_x$ | $F_z$ | $P_S$ | $P_T$ | $\Omega$ | $\Phi$ |
| Dipole model | −1.19 | −0.11 | −0.05 | 0 | 1.23 | 0.20 | 2.03 | 0.13 | 5.3 | 3.7 |

TABLE III. Dipole modulus and orientation as well as prefactor of the dipole-dipole interaction energy for Si(7 7 10) [21] and Si(1 1 15) (rebonded $D_B$ step model).

| | $P$ (nN) | $\Omega$ (deg) | $\Phi$ (deg) | $A_{el}$ (Jm) | Step height (nm) |
|---|---|---|---|---|---|
| Triple step: Si(7 7 10) [21] | 1.5 | 170 | 81 | $8 \times 10^{-30}$ | 0.94 |
| Double step: Si(001) | 2.0 | 5.3 | 3.7 | $1.1 \times 10^{-29}$ | 0.27 |

at step edges such as rebonding and its interplay with the terrace surface stress may significantly modify the equivalent elastic dipole moment at the step.

In Table III we compare the so-obtained dipole characteristics to the one we have already obtained for the Si(7 7 10) surface [a vicinal of Si(111)]. It appears that the dipole interaction is larger for double steps on vicinal Si(100) than for triple steps on vicinal Si(111). This result suggests that rebonding at double-step edges on vicinal Si(001) decreases the surface energy cost by reducing the number of dangling bonds, but at the expense of an enhancement of the local stress at the steps, giving rise here to a large stretch component of the elastic dipole.

## VI. CONCLUSION

We have shown by GIXD that the extended buried elastic dipole model can accurately describe the displacement field induced by double steps on vicinal surfaces of Si(001). The fitting of the structure factors has enabled us to determine the stretch and torque components of the elastic dipole, its lever arm, and its force orientations. We have put into evidence a large stretch component of the dipole ($2.0 \pm 0.5$ nN) localized exactly between the upper corner and the lower corner of the step. The step edge is thus highly stressed and we have calculated a stress of $3.25 \pm 0.80$ Nm$^{-1}$. This is a clear indication that if rebonding at double-layer step edges reduces the step energy, thanks to the reduction in the number of dangling bonds, it also creates a strong local stress as illustrated by the large atomic displacements in the vicinity of the step. We hope that these experimental measurements will serve as a new benchmark for further theoretical investigations of step energetics and step-step interactions on Si(001).

## ACKNOWLEDGMENTS

The authors thank G. Renaud, Nils Blanc, and the staff of the BM32 beamline of the European Synchrotron Radiation Facility (Grenoble, France). We also thank A. Ranguis for his help during the measurements of the surface morphology of Si(1 1 15) by scanning probe microscopy. This work is supported by the ANR Grant No. LOTUS (ANR-13-BS04-0004-02).

[1] A. Baski, S. Erwin, and L. Whitman, Surf. Sci. **392**, 69 (1997).
[2] B. S. Swartzentruber, Y. W. Mo, R. Kariotis, M. G. Lagally, and M. B. Webb, Phys. Rev. Lett. **65**, 1913 (1990).
[3] N. C. Bartelt, R. M. Tromp, and E. D. Williams, Phys. Rev. Lett. **73**, 1656 (1994).
[4] Y.-W. Mo, D. E. Savage, B. S. Swartzentruber, and M. G. Lagally, Phys. Rev. Lett. **65**, 1020 (1990).
[5] B. Voigtlander, Surf. Sci. Rep. **43**, 127 (2001).
[6] P. Müller and A. Saùl, Surf. Sci. Rep. **54**, 157 (2004).
[7] J. J. Métois, A. Saùl, and P. Müller, Nat. Mater. **4**, 238 (2005).
[8] F. Leroy, P. Müller, J.-J. Métois, and O. Pierre-Louis, Phys. Rev. B **76**, 045402 (2007).
[9] K. Oura, V. Lifshits, A. Saranin, A. Zotov, and M. Katayama, Surf. Sci. Rep. **35**, 1 (1999).
[10] V. Marchenko, Zh. Eksp. Teor. Fiz. **81**, 1141 (1981).
[11] V. Marchenko and A. Parshin, Zh. Eksp. Teor. Fiz. **79**, 257 (1980).
[12] G. Prévot and B. Croset, Phys. Rev. Lett. **92**, 256104 (2004).
[13] G. Prévot and B. Croset, Phys. Rev. B **74**, 235410 (2006).
[14] B. Croset and G. Prévot, Phys. Rev. B **73**, 045434 (2006).
[15] G. Prévot, A. Coati, B. Croset, and Y. Garreau, J. Appl. Crystallogr. **40**, 874 (2007).
[16] D. Chadi, Phys. Rev. Lett. **59**, 1691 (1987).
[17] T. W. Poon, S. Yip, P. S. Ho, and F. F. Abraham, Phys. Rev. B **45**, 3521 (1992).
[18] E. Pehlke and P. Kratzer, Phys. Rev. B **59**, 2790 (1999).
[19] G. Prévot, Y. Girard, V. Repain, S. Rousset, A. Coati, Y. Garreau, J. Paul, N. Mammen, and S. Narasimhan, Phys. Rev. B **81**, 075415 (2010).
[20] G. Prévot, L. Barbier, and P. Steadman, Surf. Sci. **604**, 1265 (2010).
[21] G. Prévot, F. Leroy, B. Croset, Y. Garreau, A. Coati, and P. Müller, Surf. Sci. **606**, 209 (2012).
[22] B. S. Swartzentruber, N. Kitamura, M. G. Lagally, and M. B. Webb, Phys. Rev. B **47**, 13432 (1993).
[23] O. L. Alerhand, D. Vanderbilt, R. D. Meade, and J. D. Joannopoulos, Phys. Rev. Lett. **61**, 1973 (1988).
[24] S. R. Schofield, M. W. Radny, and P. V. Smith, Phys. Rev. B **62**, 10199 (2000).
[25] I. Vilfan, Surf. Sci. **289**, L604 (1993).
[26] W. Haiss, Rep. Prog. Phys. **64**, 591 (2001).
[27] M. Payne, N. Roberts, R. Needs, M. Needels, and J. Jouannopoulos, Surf. Sci. **211/212**, 1 (1989).
[28] R. Meade and D. Vanderbilt, in *Proceedings, XX International Conference on the Physics of Semiconductors* (World Scientific, Singapore, 1990), p. 123.
[29] A. Garcia and J. E. Northrup, Phys. Rev. B **48**, 17350 (1993).
[30] Y. Umeno, A. Kushima, T. Kitamura, P. Gumbsch, and J. Li, Phys. Rev. B **72**, 165431 (2005).
[31] Y. Miyamoto, Phys. Rev. B **49**, 1947 (1994).
[32] S. Hara, S. Izumi, T. Kumagai, and S. Sakai, Surf. Sci. **585**, 17 (2005).
[33] T. Delph, Surf. Sci. **602**, 259 (2008).
[34] P. Hecquet, Surf. Sci. **639**, 1 (2015).
[35] H. J. W. Zandvliet and H. B. Elswijk, Phys Rev. B **48**, 14269 (1993).
[36] V. Cantelli, O. Geaymond, O. Ulrich, T. Zhou, N. Blanc, and G. Renaud, J. Synchrotron Radiat. **22**, 688 (2015).

[37] J. Drnec, T. Zhou, S. Pintea, W. Onderwaater, E. Vlieg, G. Renaud, and R. Felici, J. Appl. Crystallogr. **47**, 365 (2014).

[38] J. Griffith and G. Kochanski, Crit. Rev. Solid State Mater. Sci. **16**, 255 (1990).

[39] W. Press, S. Teukolsky, W. Vetterling, and B. Flannery, in *The Art of Parallel Scientific Computing* (Cambridge University Press, Cambridge, UK, 1992).

[40] G. Prévot, in *Mechanical Stress on the Nanoscale: Simulation, Materials System and Charaterization*, edited by M. Hanbücken, P. Müller, and R. Wehrspohn (Wiley-VCH, Weinheim, 2011), pp. 275–297.

[41] W. Sharpe, *MEMS Handbook, Vol. 11*, edited by M. G. el Hak (CRC Press, Boca Raton, FL, 2002), p. 829.